

The Spectral Features of Disk and Corona with Mass Evaporation in the Low/Hard State

Erlin Qiao^{1,2,3} and B.F. Liu^{1,3}.

¹ National Astronomical Observatories /Yunnan Observatory, Chinese Academy of Sciences, P.O. Box 110, Kunming 650011, P. R. China

² Graduate School of Chinese Academy of Sciences, Beijing 100049, P. R. China

³ Key Laboratory for the Structure and Evolution of Celestial Objects, Chinese Academy of Sciences

qel1982@ynao.ac.cn

bfliu@ynao.ac.cn

(Received (reception date); accepted (acceptation date))

Abstract

We investigate the spectral features of accretion flows composed of an outer cool, optically thick disk and inner hot, optically thin, advection dominated accretion flows (ADAF) within the framework of disk and corona with mass evaporation (Liu et al. 2002a). In this work, both the magnetic field and Compton scattering of soft photons from the disk by electrons in the corona are included to calculate the evaporation rates at different distances. The disk is truncated at the distance where the evaporation rate equals to the accretion rate ($\dot{m}_{\text{evap}}(r_{\text{tr}}) = \dot{m}$). For a series of accretion rates, the corresponding truncation radii are calculated out, with which we are able to calculate the emergent spectra from the inner ADAF + outer disk + corona. At very low accretion rates, the spectra are similar to that of a pure ADAF because the disk is truncated at large distances. The disk component becomes important at high accretion rates since the truncation occurs at small distances. An anti-correlation between the Eddington ratio $\xi \equiv L_{0.5-25\text{keV}}/L_{\text{Edd}}$ and the hard X-ray photon index $\Gamma_{3-25\text{keV}}$ at low/hard states is predicted by the model. Comparing the theoretical results with observations, we find that our model can reproduce the anti-correlation between the Eddington ratio ξ and the hard X-ray photon index observed for the X-ray binary XTE J1118+480.

Key words: accretion, accretion disk—stars: individual (XTE J1118+480)—X-rays: stars

1. Introduction

Accretion onto stellar black hole is the most widely accepted scenario for reproducing the different spectra in black hole X-ray binaries. Generally, there are two basic spectral states, i.e. the high/soft state and the low/hard state (Esin et al. 1997; Van de Klis 1994; Nowak 1995; Tanaka & Lewin 1995; Tanaka & Shibazaki 1996; for reviews see Remillard & McClintock 2006 and Done et al. 2007). In the high/soft state, the accretion occurs dominantly via a cool, optically thick disk (Pringle & Rees 1972; Shakura & Sunyaev 1973; Mitsuda et al. 1984; Frank et al. 2002), while in the low/hard state, the accretion dominantly via a hot, optically thin advection dominated accretion flow (ADAF) or radiative inefficient accretion flow (RIAF) (Rees et al. 1982; Narayan & Yi 1994, 1995a, b; Abramowicz et al. 1995; Narayan 2005; Kato et al. 2008). Detailed fits to the observational spectra show that in the high/soft state the disk extends to the innermost stable circular orbit (ISCO), while in the low/hard state, the disk truncates at some radius, and from the truncation radius inward the disk is replaced by an ADAF or RIAF (Kawabata & Mineshige 2010). The spectra in the low/hard state is characterized by a hard power law ($\Gamma \sim 1.5 - 2.1$) peaking at ~ 100 keV, and sometimes accompanied by a low-temperature thermal component (Esin et al. 2001; McClintock et al. 2001; Done et al. 2007). The hard power-law component is believed to be produced by the inner hot ADAF or RIAF, and the thermal component by the truncated disk (Esin et al. 2001; Done et al. 2007).

Several theoretical models are proposed to be potential mechanisms for the disk truncation in the low/hard state for black hole X-ray binaries (Honma 1996; Meyer, Liu & Meyer-Hofmeister 2000b; Manmoto & Kato 2000; Lu et al. 2004; Różańska & Czerny 2000; Spruit & Deufel 2002; Dullemond & Spruit 2005). The disk-corona evaporation model (Meyer & Meyer-Hofmeister 1994; Meyer et al. 2000a, b; Liu et al. 2002a) can naturally explain the transition between the outer thin disk and the inner ADAF/RIAF. The interaction between the disk and the corona leads to mass evaporating from the disk to the corona. When the mass accretion rate in the disk is lower than the evaporation rate from the disk to the corona, the disk is truncated. For given mass of black hole and accretion rate, the truncation radius is determined by the evaporation model. Therefore, we can calculate the radiative spectra from the inner ADAF, the outer disk and corona.

Thanks to the rapid progress of the observational techniques, more detailed data for the multi-wavelength spectra are available for studying the evolution of the truncation radius of the disk with mass accretion rate in black hole X-ray binaries (Cabanac et al. 2009). The evolution of X-ray spectra with mass accretion rate has been also investigated in both AGNs and black hole X-ray binaries (Esin et al. 1997; wang et al. 2004; Gu et al. 2009; Wu et al. 2008; Liu et al. 2009). Here, for the first time, we calculate the emergent spectra from the disk and corona, and the inner ADAF caused by the mass evaporation. We then compare the theoretical spectra of our model for different mass accretion rates with observations.

In this work, we perform more detailed calculations to study the evaporation and disk truncation in the low/hard state. Both the cooling by Compton scattering of the disk photons and the magnetic field are included to calculate the evaporation rates, which makes our solution more self-consistent. We obtain a fitting formula for the truncation radius as a function of mass accretion rates. Then, we calculate the emergent spectra from the inner ADAF, the outer disk and corona for different mass accretion rates. The dependence of the hard X-ray photon index on the mass accretion rate is derived. From the theoretical spectra, we find an anti-correlation between the Eddington ratio $\xi \equiv L_{0.5-25\text{keV}}/L_{\text{Edd}}$ and the hard X-ray photon index $\Gamma_{3-25\text{keV}}$, which is consistent with observations for the black hole X-ray binary XTE J1118+480 (Wu et al. 2008).

The paper is organized as follows. In section 2 we briefly describe the disk-corona model. In section 3 we present the numerical results, and in section 4 comparison with observations. The discussions and conclusions are given in section 5 and section 6.

2. The Model

We consider a hot corona above a geometrically thin standard disk around a central black hole. In the corona, viscous dissipation leads to ion heating, which is partially transferred to the electrons by means of Coulomb collisions. This energy is then conducted down into lower, cooler and denser corona. If the density in this layer is sufficiently high, the conductive flux is radiated away. If the density is too low to efficiently radiate the energy, cool matter is heated up and evaporation into the corona takes place. The mass evaporation goes on until an equilibrium density is established. The gas evaporating into the corona still retains angular momentum and with the role of viscosity will differentially rotate around the central object. By friction the gas loses angular momentum and drifts inward thus continuously drains mass from the corona towards the central object. This is compensated by a steady mass evaporation flow from the underlying disk. The process is driven by the gravitational potential energy released by friction in the form of heat in the corona. Therefore, mass is accreted to the central object partially through the corona (evaporated part) and partially through the disk (the left part of the supplying mass). Such a model was proposed by Meyer & Meyer-Hofmeister (1994) for dwarf novae, established for black holes by Meyer et al. (2000a) and modified by Liu et al. (2002a) where the decoupling of ions and electrons and Compton cooling effect are taken into account. Further updates by Meyer-Hofmeister & Meyer (2003), Qian et al. (2007) and Qiao & Liu (2009) are also included in this study. For clarity, we list the equations describing the physics of corona as follows.

Equation of state

$$P = \frac{\Re\rho}{2\mu}(T_i + T_e)\beta^{-1}, \quad (1)$$

where $\mu = 0.62$ is the molecular weight assuming a standard chemical composition ($X = 0.75, Y = 0.25$) for the corona, β is the ratio of gas pressure P_g to total pressure P ($P = P_g + P_m$, where P_m is magnetic pressure). For convenience, we assume the number density of ion n_i equals to that of electron

n_e , which is strictly true only for a pure hydrogen plasma.

Equation of continuity

$$\frac{d}{dz}(\rho v_z) = \eta_M \frac{2}{R} \rho v_R - \frac{2z}{R^2 + z^2} \rho v_z, \quad (2)$$

where $v_R = -\alpha \frac{V_s^2}{v_\varphi}$ is the radial component of velocity, $V_s = (\frac{P}{\rho})^{1/2}$ is the isothermal sound speed, $v_\varphi = \sqrt{\frac{GM}{r}}(1 + \frac{z^2}{r^2})^{-4/3}$ is the angular component of velocity (for the detailed derivation of v_φ , one can see Meyer et al. 2000b).

Equation of the z -component of momentum

$$\rho v_z \frac{dv_z}{dz} = -\frac{dP}{dz} - \rho \frac{GMz}{(R^2 + z^2)^{3/2}}, \quad (3)$$

The energy equation of ions

$$\begin{aligned} & \frac{d}{dz} \left\{ \rho_i v_z \left[\frac{v^2}{2} + \frac{\gamma}{\gamma-1} \frac{P_i}{\rho_i} - \frac{GM}{(R^2+z^2)^{1/2}} \right] \right\} \\ &= \frac{3}{2} \alpha P \Omega - q_{ie} \\ &+ \eta_E \frac{2}{R} \rho_i v_R \left[\frac{v^2}{2} + \frac{\gamma}{\gamma-1} \frac{P_i}{\rho_i} - \frac{GM}{(R^2+z^2)^{1/2}} \right] \\ &- \frac{2z}{R^2+z^2} \left\{ \rho_i v_z \left[\frac{v^2}{2} + \frac{\gamma}{\gamma-1} \frac{P_i}{\rho_i} - \frac{GM}{(R^2+z^2)^{1/2}} \right] \right\}, \end{aligned} \quad (4)$$

where η_M is the mass advection modification term and η_E is the energy modification term. We take $\eta_M = 1$ for the case without consideration of the effect of mass inflow and outflow from and into neighboring zones in the corona, and $\eta_E = \eta_M + 0.5$ is a modification to previous energy equations (for details see Meyer-Hofmeister & Meyer 2003). Ω is the angular velocity of the corona, $\Omega = \sqrt{\frac{GM}{r^3}}(1 + \frac{z^2}{r^2})^{-4/3}$ (for the detailed derivation of Ω , one can see Meyer et al. 2000b). q_{ie} is the exchange rate of energy between electrons and ions,

$$q_{ie} = \left(\frac{2}{\pi} \right)^{1/2} \frac{3}{2} \frac{m_e}{m_i} \ln \Lambda \sigma_T c n_e n_i (\kappa T_i - \kappa T_e) \frac{1 + T_*^{1/2}}{T_*^{3/2}}, \quad (5)$$

with

$$T_* = \frac{\kappa T_e}{m_e c^2} \left(1 + \frac{m_e T_i}{m_i T_e} \right), \quad (6)$$

where m_i and m_e are the proton and electron masses, κ is the Boltzmann constant, c is the light speed, σ_T is the Thomson scattering cross section and $\ln \Lambda = 20$ is the Coulomb logarithm.

The energy equation for both the ions and electrons

$$\begin{aligned} & \frac{d}{dz} \left\{ \rho v_z \left[\frac{v^2}{2} + \frac{\gamma}{\gamma-1} \frac{P}{\rho} - \frac{GM}{(R^2+z^2)^{1/2}} \right] + F_c \right\} \\ &= \frac{3}{2} \alpha P \Omega - n_e n_i L(T) - q_{\text{Comp}} \\ &+ \eta_E \frac{2}{R} \rho v_R \left[\frac{v^2}{2} + \frac{\gamma}{\gamma-1} \frac{P}{\rho} - \frac{GM}{(R^2+z^2)^{1/2}} \right] \\ &- \frac{2z}{R^2+z^2} \left\{ \rho v_z \left[\frac{v^2}{2} + \frac{\gamma}{\gamma-1} \frac{P}{\rho} - \frac{GM}{(R^2+z^2)^{1/2}} \right] + F_c \right\}, \end{aligned} \quad (7)$$

where $n_e n_i L(T)$ is the bremsstrahlung cooling rate and F_c is the thermal conduction (Spitzer 1962),

$$F_c = -\kappa_0 T_e^{5/2} \frac{dT_e}{dz}, \quad (8)$$

with $\kappa_0 = 10^{-6} \text{erg s}^{-1} \text{cm}^{-1} \text{K}^{-7/2}$ for fully ionized plasma. q_{Comp} is the Compton cooling rate,

$$q_{\text{Comp}} = \frac{4\kappa T_e}{m_e c^2} n_e \sigma_T c \frac{a T_{\text{eff}}^4}{2}, \quad (9)$$

with T_{eff} the effective temperature of the underlying thin disk and a the radiation constant.

$$T_{\text{eff}} = \frac{3GM\dot{M}_d}{8\pi R^3\sigma}, \quad (10)$$

where $\dot{M}_d(R)$ is the mass accretion rate in the thin disk, which depends on the distance because of evaporation,

$$\dot{M}_d(R) = \dot{M} - \dot{M}_{\text{evap}}(R), \quad (11)$$

With \dot{M} the mass transfer rate from the secondary, which is assumed equal to the mass accretion rate in the most outer region of the accretion disk and \dot{M}_{evap} the integrated evaporation rate from the outer edge of the disk to the distance R .

All other parameters in above equations are under standard definitions, and are in cgs units. The five differential equations, Eqs. (2), (3), (4), (7), (8), which contain five variables $P(z)$, $T_i(z)$, $T_e(z)$, $F_c(z)$, and $\dot{m}(z) (\equiv \rho v_z)$ can be solved with five boundary conditions.

At the lower boundary z_0 (the interface of disk and corona), the temperature of the gas should be the effective temperature of the accretion disk. Previous investigations (Liu, Meyer, & Meyer-Hofmeister 1995) show that the coronal temperature increases from effective temperature to $10^{6.5}\text{K}$ in a very thin layer and thus the lower boundary conditions can be reasonably approximated (Meyer et al. 2000a; Qian et al. 2007) as,

$$\begin{aligned} T_i &= T_e = 10^{6.5}\text{K}, \\ F_c &= -2.73 \times 10^6 \beta P \text{ at } z = z_0. \end{aligned} \quad (12)$$

At infinity, there is no pressure and no heat flux. This requires sound transition at some height $z = z_1$. We then constrain the upper boundary as,

$$F_c = 0 \text{ and } v_z = V_s \text{ at } z = z_1. \quad (13)$$

With such boundary conditions, we assume a set of lower boundary values for P and \dot{m} to start the integration along z . Only when the trial values for P and \dot{m} fulfill the upper boundary conditions can the presumed P and \dot{m} be taken as true solutions of the differential equations.

3. Numerical Results

In our calculation we fix the central black hole mass as $M = 6M_\odot$, viscosity parameter as $\alpha = 0.3$, and assume equipartition of gas pressure and magnetic pressure, i.e., $\beta = 0.5$. The evaporation rate is calculated from the vertical mass flow at the lower boundary, $\dot{m}_0 \equiv \rho v_z$, and is then integrated in the radial one-zone region, $\dot{M}_{\text{evap}} \approx 2\pi R^2 \dot{m}_0$. This integrated evaporation rate represents the mass flowing rate in the local corona if there is no gas supply except for the mass transfer from the secondary in a binary system. If the mass transfer rate \dot{M} is less than the maximum evaporation rate, the thin disk will truncate at the radius R_{tr} where the accretion rate equals to the evaporation rate. The region from the truncation radius inward is filled with a hot ADAF and the region from the truncation radius outward there is a thin disk, above which there is a hot corona providing the material for the ADAF. If the mass transfer rate \dot{M} is higher than the maximal evaporation rate, the thin

disk will extend down to the ISCO, only a very weak corona exists above the thin disk.

3.1. The Evaporation Features and Disk Truncation

Figure 1 shows the evaporation curves for different mass accretion rates. Here the evaporation rate is scaled with the Eddington accretion rate, $\dot{M}_{\text{Edd}} = L_{\text{Edd}}/\eta c^2 = 1.39 \times 10^{18} M/M_\odot \text{ g s}^{-1}$ (where $\eta = 0.1$ is the energy conversion efficiency) and the radius is scaled with the Schwarzschild radius, $R_S = 2GM/c^2 = 2.95 \times 10^5 M/M_\odot \text{ cm}$. As the first step, we neglect the effect of Compton cooling in the corona associated with soft photons emitted by the underlying thin disk. The evaporation rate without Compton cooling is shown by the solid curve in Figure 1. Taking into account the Compton effect, we calculate the evaporation rates for a series of accretion rates. For $\dot{M} = 0.005 \dot{M}_{\text{Edd}}$, the evaporation curve is almost the same as the case without considering the Compton cooling, which can be seen from Figure 1 for the long-dashed line. We get an analytical formula between the mass accretion rate and the truncation radius by fitting the numerical results without Compton cooling, which is suitable for the case of $\dot{M} < 0.005 \dot{M}_{\text{Edd}}$, that is,

$$r_{\text{tr}} = 2.215 \dot{m}^{-0.776} \quad (14)$$

where \dot{m} is scaled with Eddington accretion rate and r_{tr} is scaled with Schwarzschild radius. Using this formula, the truncation radius is $200 R_S$ for $\dot{M} = 0.003 \dot{M}_{\text{Edd}}$ and $471 R_S$ for $\dot{M} = 0.001 \dot{M}_{\text{Edd}}$ respectively.

With increase of the mass accretion rate, the evaporation is suppressed by the strong Compton cooling. For $\dot{M} = 0.008 \dot{M}_{\text{Edd}}$, the evaporation curve deviates the case without considering the Compton cooling, and the evaporation rate becomes weaker. However, the deviation is slight and the thin disk truncates at around $78.5 R_S$, which is not quite different from the case without the Compton cooling, one can see the dot-dashed line from Figure 1. Increasing the mass accretion rate further to $\dot{M} = 0.01 \dot{M}_{\text{Edd}}$, the evaporation becomes very weak, and the thin disk truncates at a relative small radius $40 R_S$. For clarity, we show the relation between the mass accretion rate and the truncation radius with the Compton cooling of the soft photos from the thin disk to the corona in Figure 2. The truncated disk corona plus ADAF geometry described above corresponds to the low/hard state.

In order to check whether the inner ADAF solution can connect with the outer disk-corona solution smoothly, we take $\dot{M} = 0.01 \dot{M}_{\text{Edd}}$ as an example to demonstrate the distribution of the temperature along radial direction. The thin disk truncates at about $40 R_S$ for $\dot{M} = 0.01 \dot{M}_{\text{Edd}}$. From Figure 3, we can see the ion temperature of the outer corona connect with the inner ADAF well (the dashed line). The radial distribution of ion temperature is similar to the virial temperature ($T_i \propto R^{-1}$) (the solid line). However, the electron temperature of the outer corona is lower than that of the inner ADAF (the dotted line). This can be understood as follows. Because of the presence of the cool thin disk underneath, the cooling of the corona by electron thermal conduction between the corona and the underlying thin disk is much more efficient than that of the radiative cooling, thereby leads to a lower electron temperature of the corona than that of the ADAF.

With increase of the mass accretion rate further for $\dot{M} = 0.011 \dot{M}_{\text{Edd}}$, the evaporation rate decreases severely. Because the peak value of the evaporation rate is less than $0.011 \dot{M}_{\text{Edd}}$, the thin disk extends to the ISCO, and only a weak corona exists above the disk. we can see the dotted line from Figure 1. This configuration corresponds to the high/soft state, and this accretion rate corresponds to the critical accretion rate between the low/hard state and high/soft state transition. We note that the critical accretion rate $\dot{M} = 0.011 \dot{M}_{\text{Edd}}$ is less than the previous result, $\dot{M} \approx 0.03 \dot{M}_{\text{Edd}}$, from our model for $\alpha = 0.3$ (Meyer et al. 2000a, b; Liu et al. 2002a; Qiao & Liu 2009). This is because the Compton cooling of the soft photons from the thin disk to the corona is considered. The inverse Compton scattering will make the cooling in the corona more efficient, and then suppresses the evaporation, thereby leading to a relative smaller evaporation rate.

3.2. The Spectra of Disk and Corona in the Low State

If $\dot{M} < 0.01 \dot{M}_{\text{Edd}}$, the thin disk is truncated by mass evaporation. With determination of truncation radius as described in section 3.1, we can calculate the emergent spectra from the inner ADAF/RIAF and outer disk and corona. We describe the ADAF/RIAF by the self-similar solution (Narayan et al. 1994, 1995b), and the region from the truncation radius outward by two phase disk-corona accretion flows. The physical quantities for calculating the emergent spectra are the distribution of the density ρ , Thomson scattering optical depth τ_{es} and electron temperature T_e along radial direction. The contribution of the accretion flows to the spectra includes two parts, the inner ADAF/RIAF and the outer disk and corona.

For the inner ADAF, we follow the work of Narayan et al. (1995b). The density ρ and electron Thomson scattering optical depth τ_{es} are,

$$\begin{aligned} \rho &= 3.79 \times 10^{-5} \alpha^{-1} c_1^{-1} c_3^{-1/2} m^{-1} \dot{m} r^{-3/2} \text{ g cm}^{-3}, \\ \tau_{\text{es}} &= 12.4 \alpha^{-1} c_1^{-1} \dot{m} r^{-1/2}, \end{aligned} \quad (15)$$

where

$$\begin{aligned} c_1 &= \frac{(5+2\varepsilon')}{3\alpha^2} g(\alpha, \varepsilon'), \\ c_3 &= \frac{2\varepsilon(5+2\varepsilon')}{9\alpha^2} g(\alpha, \varepsilon'), \\ \varepsilon' &= \frac{\varepsilon}{f} = \frac{1}{f} \left(\frac{5/3-\gamma}{\gamma-1} \right), \\ g(\alpha, \varepsilon') &= \left[1 + \frac{18\alpha^2}{(5+2\varepsilon')^2} \right]^{1/2} - 1, \\ \gamma &= \frac{32-24\beta-3\beta^2}{24-21\beta}, \end{aligned} \quad (16)$$

with f the fraction of viscosity dissipated energy which is advected. The energy equation of ions, electrons and the state equation are (Narayan et al. 1995b),

$$\begin{aligned} q^+ &= f q^+ + q^{\text{ie}} \\ q^{\text{ie}} &= q^- \\ T_i + 1.08 T_e &= 6.66 \times 10^{12} \beta c_3 r^{-1}, \end{aligned} \quad (17)$$

where q^+ is the viscous dissipation of energy per unit volume,

q^{ie} is the exchange rate of energy between electrons and ions per unit volume, and q^- is the cooling rate of the electrons per unit volume. The expression of q^+ , q^{ie} and q^- can be found in Narayan et al (1995b), i.e.,

$$\begin{aligned} q^+ &= 1.84 \times 10^{21} \varepsilon' c_3^{1/2} m^{-2} \dot{m} r^{-4} \text{ ergs cm}^{-3} \text{ s}^{-1}, \\ q^{\text{ie}} &= 5.61 \times 10^{-32} \frac{n_e n_i (T_i - T_e)}{K_2(1/\theta_e) K_2(1/\theta_i)} \\ &\quad \times \left[\frac{2(\theta_e + \theta_i)^2 + 1}{(\theta_e + \theta_i)} K_1 \left(\frac{\theta_e + \theta_i}{\theta_e \theta_i} \right) + 2K_0 \left(\frac{\theta_e + \theta_i}{\theta_e \theta_i} \right) \right] \text{ ergs cm}^{-3} \text{ s}^{-1}, \\ q^- &= q_{\text{bresm}}^- + q_{\text{synch}}^- + q_{\text{bresm,c}}^- + q_{\text{synch,c}}^- + q_{\text{disk,c}}^-. \end{aligned} \quad (18)$$

where the K 's are modified Bessel functions, q_{bresm}^- , q_{synch}^- , $q_{\text{bresm,c}}^-$, $q_{\text{synch,c}}^-$, $q_{\text{disk,c}}^-$ are the bremsstrahlung cooling rate, synchrotron radiation rate, the cooling rate by the Comptonization of bremsstrahlung radiation, synchrotron radiation and the soft photons emitted by the outer disk. Given α , β , m , \dot{m} and r , we can calculate the coronal quantities T_e , T_i , ρ , τ_{es} from equation (15) to equation (18). Here, for the electron radiation cooling term q^- , we add the soft photons which come from the outer truncated thin disk to be scattered by electrons in the inner ADAF. This cooling term is determined by the size of the truncation radius of the thin disk, which can be obtained from our calculation as described in section 3.1. With ρ , τ_{es} and T_e determined, we can calculate the emergent spectra from the inner ADAF.

As the first step, we calculate the Bremsstrahlung and synchrotron radiation from the inner ADAF. Adopting the Eddington approximation and the two-stream approximation (Rybicki & Lightman 1979; Manmoto et al. 1997), the radiative diffusion equation in the vertical direction is solved, and the radiative flux is given by

$$F_\nu = \frac{2\pi}{\sqrt{3}} B_\nu [1 - \exp(-2\sqrt{3}\tau_\nu^*)], \quad (19)$$

where B_ν is the plank function, $\tau_\nu^* = (\pi^{1/2}) \kappa_\nu H$ is the vertical absorption optical depth. Assuming local thermodynamic equilibrium (LTE), we can write $\kappa_\nu = \chi_\nu / 4\pi B_\nu$, $\chi_\nu = \chi_{\nu, \text{bresm}} + \chi_{\nu, \text{synch}}$ is the total emissivity, $\chi_{\nu, \text{bresm}}$ the bremsstrahlung emissivity and $\chi_{\nu, \text{synch}}$ the synchrotron emissivity (for the detailed expression for $\chi_{\nu, \text{bresm}}$ and $\chi_{\nu, \text{synch}}$ see Narayan et al. 1995b). Photons emitted in the Bremsstrahlung and synchrotron processes can be scattered by electrons in the ADAF (self-Compton scattering). With known spectra of soft photons (equation (19)) and ADAF structure (T_e and τ_{es}), we calculate the local Compton scattering spectra in terms of multi-scattering method (Coppi & Blandford 1990). We integrate this local Compton radiative spectra from the ISCO to the truncation radius R_{tr} and get the whole emergent spectra of the inner ADAF. The method we used here separates the inverse Compton scattering process from other emission and absorption processes. Because the optical depth is relative small ($\tau < 1$), this treatment is a good approximation.

For the outer disk corona, we get the density ρ , Thomson scattering optical depth τ_{es} and electron temperature T_e of the corona from the self-consistent calculation of the disk-corona as described in section 2. For the disk corona in the vertical direction, there is a thin transition layer between the cool thin disk and the hot corona. The temperature of the transition layer

is about $10^{6.5}$ K, and the optical depth is relative small, so we neglect the Compton radiation from this layer. Because of the existence of the underlying thin disk, we add the soft photons flux $F_{\nu, \text{disk}}$ from the thin disk as the initial seed photon flux for the inverse Compton scattering. The total seed photon flux for the inverse Compton scattering is,

$$F_{\nu} = \frac{2\pi}{\sqrt{3}} B_{\nu} [1 - \exp(-2\sqrt{3}\tau_{\nu}^*)] + F_{\nu, \text{disk}}, \quad (20)$$

where $F_{\nu, \text{disk}} = \pi I_{\nu} = \pi B_{\nu}(T_{\text{eff}})$, $T_{\text{eff}} = \left\{ \frac{3GM\dot{M}_d}{8\pi R^3\sigma} \left[1 - \sqrt{\frac{R_{\text{tr}}}{R}} \right] \right\}^{1/4}$, Using the same method we have described for the ADAF to treat the Comptonization process, we get the local spectra of the disk and corona at given distance, then we start the integration from truncation radius R_{tr} to the outer boundary of the accretion disk ($\sim 3000 R_S$) to obtain the whole emergent spectra of the outer disk and corona.

Combining the contribution of both the inner ADAF and the outer disk and corona, we get the total emergent spectra of our model. The spectra are plotted in Figure 4 for mass accretion rates $\dot{M} = 0.001, 0.003, 0.005, 0.008, 0.01 \dot{M}_{\text{Edd}}$. For a lower mass accretion rate $\dot{M} = 0.001 \dot{M}_{\text{Edd}}$, the disk truncates at $471 R_S$. Because of the large truncation radius, the radiation from the inner ADAF dominates over that of the outer disk and corona, as shown by the dotted curve in the first panel of Figure 5. The first peak of this spectrum is dominated by the self-absorbed synchrotron radiation of the ADAF. The hard X-ray spectra is dominated by the thermal bremsstrahlung of the ADAF. For $\dot{M} = 0.003 \dot{M}_{\text{Edd}}$, the spectrum is plotted in the upper, right panel of Figure 5. The thin disk moves inwards and truncates at around $200 R_S$. In this case, the radiation from the inner ADAF still dominates over that of the outer disk and corona. However, the contribution of the truncated disk and corona to the first peak of the spectrum increases, and the Compton radiation of the ADAF becomes more important for the hard X-ray spectrum. With increase of the mass accretion rate, say, for $\dot{M} = 0.008, 0.01 \dot{M}_{\text{Edd}}$, the thin disk moves inwards further, and truncates at $78.5 R_S, 40 R_S$ respectively. The first peak of the spectra is dominated by the radiation from the truncated disk, and the second peak around 100 keV in X-ray band is dominated by the Compton radiation of the inner ADAF, as shown by the lower panels of Figure 5. Here, we note that although the truncation radius is small ($40 R_S$) for $\dot{M} = 0.01 \dot{M}_{\text{Edd}}$, the emission of ADAF is still more luminous than that of lower \dot{M} with large truncation radius. This can be understood as, firstly, the luminosity of ADAF is proportional to \dot{M}^2 , so with increase of the accretion rate the luminosity increases; secondly, most potential energy of ADAF is released in the most inner region around the black hole within the framework of ADAF self-similar solution.

The variation of the hard X-ray spectra with the mass accretion rates is plotted in Figure 6. We demonstrate that the hard X-ray photon index $\Gamma_{3-25 \text{ keV}}$ is anti-correlated with the mass accretion rate. This is because, with increase of the accretion rate, the Comptonization of the synchrotron and bremsstrahlung photons by the hot electrons becomes dominant. Therefore, the Thomson optical depth and hence

Compton y -parameter increases, resulting in a harder X-ray spectra.

If $\dot{M} > 0.01 \dot{M}_{\text{Edd}}$, the thin disk extends down to the ISCO, and above the thin disk only a weak corona exists as a consequence of strong external Compton scattering. The emission property in this case will be studied in the future.

4. Comparison with XTE 1118+480

Observation shows there is a strong anti-correlation between the Eddington ratio ξ and the hard X-ray photon index Γ for the black hole X-ray binary XTE 1118+480 at low Eddington ratio $\xi < 0.01$. We compare this correlation with the prediction of disk and corona model.

McClintock et al. (2001) and Wagner et al. (2001) independently confirmed the orbital period to be 4.1 hr (as previously suggested by Cook et al. 2000; Patterson 2000; Uemura et al. 2000; Dubus et al. 2001) and determined the value of the mass function to be $f(M) \simeq 6.0 M_{\odot}$ (Esin et al. 2001). The distance was estimated to be 1.8 ± 0.6 kpc (McClintock et al. 2001) and was taken as $d = 2.9$ kpc to model the multi-wavelength spectrum (Esin et al. 2001). By taking $M = 6 M_{\odot}$, viscosity parameter $\alpha = 0.3$, the ratio of gas pressure to total pressure $\beta = 0.5$, we show our theoretical relation between the Eddington ratio $\xi \equiv L_{0.5-25 \text{ keV}}/L_{\text{Edd}}$ and the hard X-ray photon index $\Gamma_{3-25 \text{ keV}}$ in Figure 7 for a series of accretion rate $\dot{M} = 0.001, 0.003, 0.005, 0.008, 0.01 \dot{M}_{\text{Edd}}$. The pluses are the observational data (Wu et al. 2008) for taking the black hole mass as $M = 6 M_{\odot}$, and the distance $d = 2.9$ kpc (Esin et al. 2001) (Note: We get the observational data from Wu et al. (2008). In the work of Wu et al. (2008) the black hole mass $M = 6.1 M_{\odot}$ and the distance $d = 1.8$ kpc are adopted to obtain ξ . We recalculate the value of ξ by taking $M = 6 M_{\odot}$ and the distance $d = 2.9$ kpc). Because ξ is related to the distance, we take different estimated distance for comparisons. The diamonds are for $d = 1.8 + 0.6$ kpc (McClintock et al. 2001), and the pluses for $d = 1.8$ kpc (Wu et al. 2008). One can see our theoretical results for the bigger distance $d = 2.9$ kpc can fit the observational data better than that of $d = 1.8$ kpc. Due to the uncertainty of the measurement to the distance, our theoretical result can only reproduce this tendency of anti-correlation to some extent.

5. Discussion

5.1. The Effect of the Viscosity Parameter and the Ratio of Magnetic Pressure to Gas Pressure

Throughout our calculations, the viscosity parameter and the ratio of magnetic pressure to gas pressure are fixed to $\alpha = 0.3$ and $\beta = 0.5$. Varying these parameters leads to a change of truncation radius at any given accretion rate (Qian et al. 2007; Qiao & Liu 2009). Nevertheless, the spectrum is only slightly affected by the truncation radius since the total emitted spectrum is dominated by the inner ADAF, in particularly in the case of large truncation radii. Only when the truncation radius is as small as $\sim 10 R_S$, where the Compton cooling of the soft photons from the outer disk to the ADAF becomes the dominated cooling mechanism, can the spectral index be largely affected. However, such a small truncation radius is very difficult

to reach according to our model.

The viscosity parameter can also affect the critical transition rate (Meyer-Hofmeister et al. 2001; Qiao & Liu 2009). For a larger value, $\alpha > 0.3$, the hard state extends to higher accretion rates, $\dot{m} > 0.01$. In this case, the distribution of photon index as a function of accretion rate, as shown in Figure 6, cannot be changed much at low accretion rates ($\dot{m} < 0.01$) or low luminosities since the truncation radius is large and hence the emitting spectrum is dominated by the inner ADAF. However, at high accretion rates (from $\dot{m} = 0.01$ up to the state transition rate), the disk is truncated at smaller radii, which could result in softer photon index than that shown in Figure 6. For a smaller viscosity, $\alpha < 0.3$, the disk is truncated at larger distances. The spectrum is hardly affected at any given accretion rates. Only the lower limit of the photon index (see figure 6) is larger because the predicted transition rate is lower.

5.2. The Challenge to the Disk Truncation

The observation of XTE J1650-500 (Miller et al. 2002; Miniutti et al. 2004) and GX 339-4 (Miller et al. 2006a; b) demonstrates that the smeared iron line and reflection feature in the low/hard state are inconsistent with disk truncation. The claimed broadening and skewed iron line, which may be caused by the Doppler shift and strong general relativistic effect, require that the thin disk extends to the ISCO (Fabian et al. 2000; Miller 2007; Done et al. 2007). Recently, the condensation of matter from a hot corona to a cool, optically thick innermost disk is proposed for black hole transient systems in the low/hard state (Meyer et al. 2007; Liu et al. 2007; Taam et al. 2008). This model may alleviate the contradiction that a thin disk exists near ISCO in the low/hard state. Present observational technique can not directly diagnose whether the thin disk truncates at some radius or not (Young et al. 2000; Gierliński et al. 1997). Further more advanced instruments are expected to solve this problem.

6. Conclusion

In this work, we investigate the spectral features of accretion flows composed of an outer cool, optically thick disk and inner hot, optically thin, advection dominated accretion flows (ADAF) within the framework of disk and corona with mass evaporation. The disk is truncated at the distance where the evaporation rate equals to the accretion rate ($\dot{m}_{\text{evap}}(r_{\text{tr}}) = \dot{m}$). We show the disk evaporation mechanism can connect the outer disk and the inner ADAF/RIAF smoothly. We calculate the emergent spectra of the disk and corona with mass evaporation in the low/hard state for different mass accretion rates. From the theoretical spectra, we find an anti-correlation between the Eddington ratio $\xi = L_{0.5-25\text{keV}}/L_{\text{Edd}}$ and the hard X-ray photon index $\Gamma_{3-25\text{keV}}$, which agrees well with the observations for the black hole X-ray binary XTE J1118+480.

We would like to thank Marat Gilfanov, F. Meyer and E. Meyer-Hofmeister for their promising discussion. Erlin Qiao thanks the support of Doctoral Promotion Program between Chinese Academy of Sciences and Max Planck Society. In addition, this work is supported by the National Nature Science Foundation of China (grants 10533050 and 10773028) and by

the National Basic Research Program of China-973 Program 2009CB824800.

References

- Abramowicz, Marek A., Chen, Xingming, Kato, Shoji, Lasota, Jean-Pierre, & Regev, Oded 1995, *ApJ*, 438, 37
- Cabanac, C., Fender, R. P., Dunn, R. J. H., & Krding, E. G., 2009, *MNRAS*, 396, 1415
- Cao, xinwu 2008, *MNRAS*, 394, 207
- Cook, L., Patterson, J., Buczynski, D. & Fried, R., 2001, *IAU Circ.* 7397
- Coppi, P. S., & Blandford, R. D. 1990, *MNRAS*, 245, 453
- Davis, Shane W., Done, Chris, & Blaes, Omer M. 2006, *ApJ*, 647, 525
- Done, C., Gierliński, Marek, & Kubota, Aya 2007, *A&A Rev.*, 15, 1
- Dubus, Guillaume, Kim, Rita S. J., Menou, Kristen, Szkody, Paula & Bowen, David V. 2001, *ApJ*, 553, 307
- Dullemond, C. R., & Spruit, H. C. 2005, *A&A*, 434, 415
- Esin, A. A, McClintock J. E., & Narayan, R. 1997, *ApJ*, 489, 865
- Esin, A. A, McClintock, Jeffrey E., Drake, Jeremy J., Garcia, Michael R., Haswell, Carole A., Hynes, Robert I., & Munro, Michael P. 2001, *ApJ*, 555, 483
- Fabian, A. C., Iwasawa, K., Reynolds, C. S., & Young, A. J. 2000 *PASP*, 112, 1145
- Frank, J., King, A., & Raine, D. 2002, *Accretion Power in Astrophysics*, Cambridge Univ. Press
- Gierliński M., Zdziarski A. A., Done C., Johnson W. N., Ebisawa K., Ueda Y., Haard F., & Philps B. F. 1997, *MNRAS*, 288, 958
- Kato, S. Fukue, J. & Mineshige, S. 2008, "Black-Hole Accretion Disks", Kyoto University Press (Kyoto)
- Kawabata, Ryoji, & Mineshige, Shin, 2010, preprint(astro-ph/1003.1430)
- Gu, Minfeng, & Cao, Xinwu, 2009, *MNRAS*, 399, 349
- Honma, F. 1996, *PASJ*, 48, 77
- Liu, B. F., Mineshige, S., Meyer, F., Meyer-Hofmeister, E., & Kawaguchi, T. 2002a, *ApJ*, 575, 117
- Liu, B. F., Mineshige, S., & Shibata, K. 2002b, *ApJ*, 572, 173
- Liu, B. F., Mineshige, S., & Ohsuga, K. 2003, *ApJ*, 587, 571
- Liu, B. F., Taam, R. E., Meyer, F., & Meyer-Hofmeister, E. 2007, *ApJ*, 671, 695
- Liu, F. k., Meyer, F., & Meyer-Hofmeister, E., 1995, *A&A*, 300, 823
- Liu, Jie-Ying, & Liu, Bi-Fang, 2009, *RAA*, 9, 966L
- Lu, Ju-Fu, Lin, Yi-Qing, & Gu, Wei-Min 2004, *ApJ*, 602, L37
- Mahadevan, Rohan 1997, *ApJ*, 477, 585
- McClintock, J. E., Garcia, M. R., Caldwell, N., Falco, E. E., Garnavich, P. M., & Zhao, P. 2001, *ApJ*, 551, 147
- Manmoto, T., & Kato, S. 2000, *ApJ*, 538, 295
- Manmoto, T., Mineshige, S., & Kusunose, M. 1997, *ApJ*, 489, 791
- Miller et al. 2002, *MNRAS*, 329, 69M
- Miller, J. M., 2007, *ARA&A*, 45, 441
- Miller, J. M., Homan, J., & Miniutti, G. 2006a, *ApJ*, 652, L113
- Miller, J. M., Homan, J., Steeghs, D., Rupen, M., Hunstead, R. W., Wijnands, R., Charles, P. A., & Fabian, A. C., 2006b, *ApJ*, 653, 525
- Miniutti, G., Fabian, A. C., & Miller, J. M., 2004, *MNRAS*, 351, 466M
- Meyer, F., & Meyer-Hofmeister, E. 1994, *A&A*, 288, 175
- Meyer, F., Liu, B. F., & Meyer-Hofmeister, E. 2000a, *A&A*, 361, 175
- Meyer, F., Liu, B. F., & Meyer-Hofmeister, E. 2000b, *A&A*, 354, L67
- Meyer, F., & Meyer-Hofmeister, E., 2002, *A&A*, 392, 5
- Meyer, F., Liu, B. F., & Meyer-Hofmeister, E. 2007, *A&A*, 463, 1
- Meyer-Hofmeister, E., & Meyer, F., 2001, *A&A*, 380, 739
- Meyer-Hofmeister, E., & Meyer, F., 2003, *A&A*, 402, 1013

- Mitsuda, K., Inoue, H., Koyama, K., Makishima, K., Matsuoka, M.,
Ogawara, Y., Suzuki, K., Tanaka, Y., Shibazaki, N., & Hirano, T.
1984, PASJ, 36, 741
- Narayan, R., & Yi, I. 1994, ApJ, 428, L13
- Narayan, R., & Yi, I. 1995a, ApJ, 444, 231
- Narayan, R., & Yi, I. 1995b, ApJ, 452, 710
- Narayan, R. 1996, ApJ, 462, 136
- Narayan, R. 2005, Ap&SS, 300, 177
- Nowak, M. A. 1995, PASP, 107, 1207
- Patterson, J., 2000, IAU Circ., 7412
- Pringle, J. E., & Rees, M. J. 1972, A&A, 21, 1
- Qian, Lei, Liu, B. F., & Wu, Xue-Bing 2007, ApJ, 668, 1145
- Qiao, Erlin, & Liu, B. F. 2009, PASJ, 61, 403
- Remillard, Ronald A., & MacClintock, Jeffrey E. 2006, ARA&A, 44,
49
- Rees, M. J., Belgman, M. C., Blandford, R. D., & Phinney, E. S. 1982,
Nature, 295, 17
- Różańska, A., & Czerny, B. 2000, A&A, 360, 1170
- Rybicki, George B., & Lightman, Alan P., 1979, Radiative Processes
in Astrophysics (New York: Wiley)
- Shakura, N. I., & Sunyaev, R. A. 1973, A&A, 24, 337
- Spitzer, L. 1962, Physics of Fully Ionized Gases, 2nd edition,
Interscience Publ., New York, London
- Spruit, H. C., & Deufel, B. 2002, A&A, 387, 918
- Taam, Ronald E., Liu, B. F., Meyer, F., & Meyer-Hofmeister, E. 2008,
ApJ, 688, 527
- Tanaka, Y., & Lewin W. H. G. 1995, X-ray binary, ed Lewin, W. H.
G. et al. (Cambridge: Cambridge Univ. Press), 126
- Tanaka, Y., & Shibazaki 1996, ARA&A, 34, 607
- Uemura, Makoto et al., 2000, PASJ, 52, L15
- Van der Klis 1994, ApJS, 92, 511
- Wang, Jian-Min, Ken-Ya Watarai, & Shin Mineshige, 2004, ApJ, 607,
107
- Wagner, R. Mark, Foltz, C. B., Shahbaz, T., Casares, J., Charles, P.
A., Starrfield, S. G., & Hewett, P. 2001, ApJ, 556, 42
- Wu, Qingwen, & Gu, Mingfeng 2008, ApJ, 682, 212
- Young, A. J., & Reynolds, C. S. 2000, ApJ, 529, 101

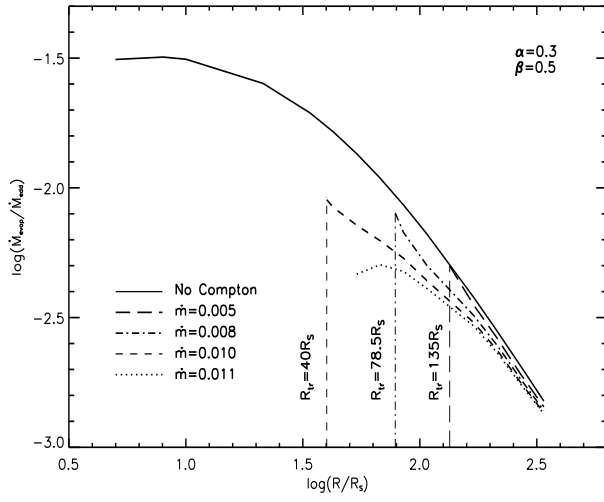


Fig. 1. The evaporation rates along radial direction for different mass accretion rates. The solid curve corresponds to the evaporation rate without Compton cooling of the soft photons emitted by the thin disk. The long-dashed line denotes the evaporation rate distribution along the radial direction for $\dot{M} = 0.005 \dot{M}_{\text{Edd}}$, the dot-dashed line for $\dot{M} = 0.008 \dot{M}_{\text{Edd}}$, the short-dashed line for $\dot{M} = 0.01 \dot{M}_{\text{Edd}}$, and the dotted line for $\dot{M} = 0.011 \dot{M}_{\text{Edd}}$. For $\dot{M} = 0.005 \dot{M}_{\text{Edd}}$, $\dot{M} = 0.008 \dot{M}_{\text{Edd}}$ and $\dot{M} = 0.01 \dot{M}_{\text{Edd}}$ the thin disk truncates at around $135 R_S$, $78.5 R_S$ and $40 R_S$ respectively. For $\dot{M} = 0.011 \dot{M}_{\text{Edd}}$, the thin disk extends to the ISCO. In our calculation, $M = 6M_{\odot}$, $\alpha = 0.3$ and $\beta = 0.5$ are adopted.

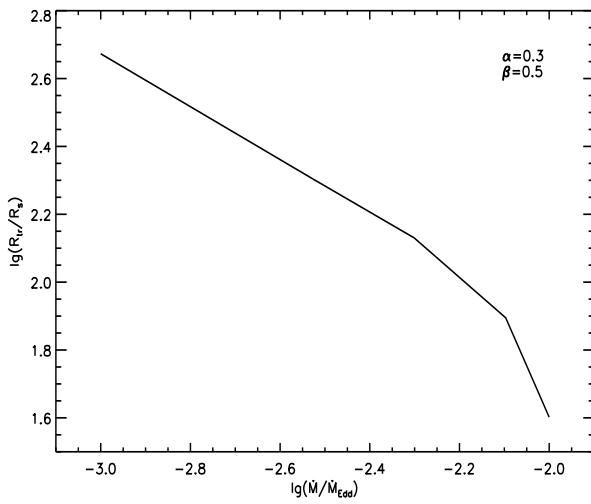


Fig. 2. The dependence of the truncation radius on the mass accretion rate. $M = 6M_{\odot}$, $\alpha = 0.3$ and $\beta = 0.5$ are adopted.

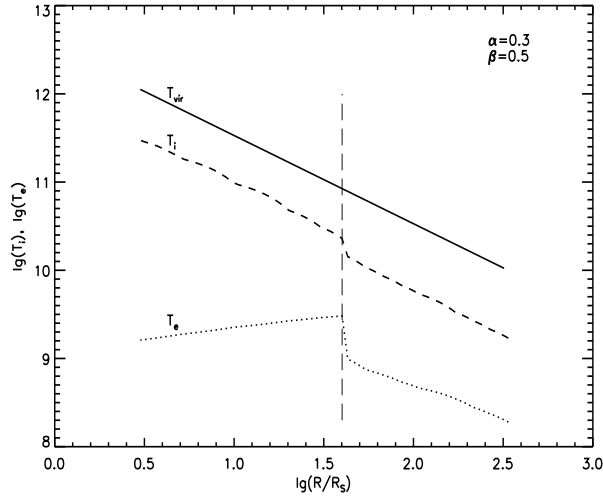


Fig. 3. The temperature versus the distance from the black hole for $\dot{M} = 0.01 \dot{M}_{\text{Edd}}$. The solid line is for the virial temperature. The dashed line and the dotted line are the ion temperature and the electron temperature distribution respectively. The lines in the left part of the vertical long-dashed line is for the inner self-similar solution of ADAF, and the right part is for the outer corona solution. $M = 6M_{\odot}$, $\alpha = 0.3$ and $\beta = 0.5$ are adopted.

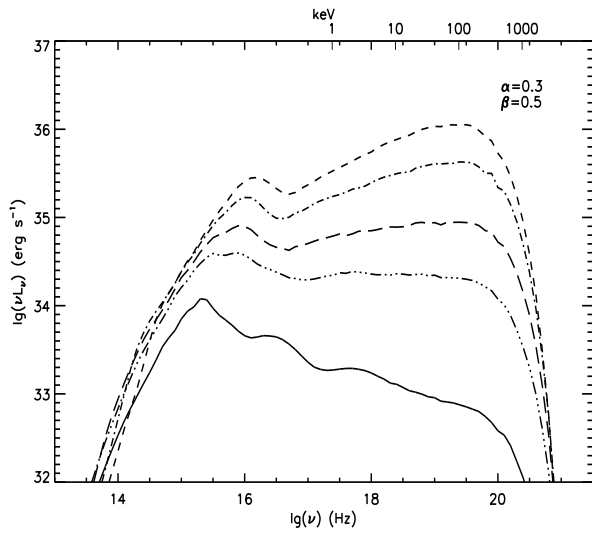


Fig. 4. The emergent spectra of disk and corona with mass evaporation. The curves from the bottom up are the emergent spectra for $\dot{M} = 0.001, 0.003, 0.005, 0.008, 0.01 \dot{M}_{\text{Edd}}$ respectively. $M = 6M_{\odot}$, $\alpha = 0.3$ and $\beta = 0.5$ are adopted.

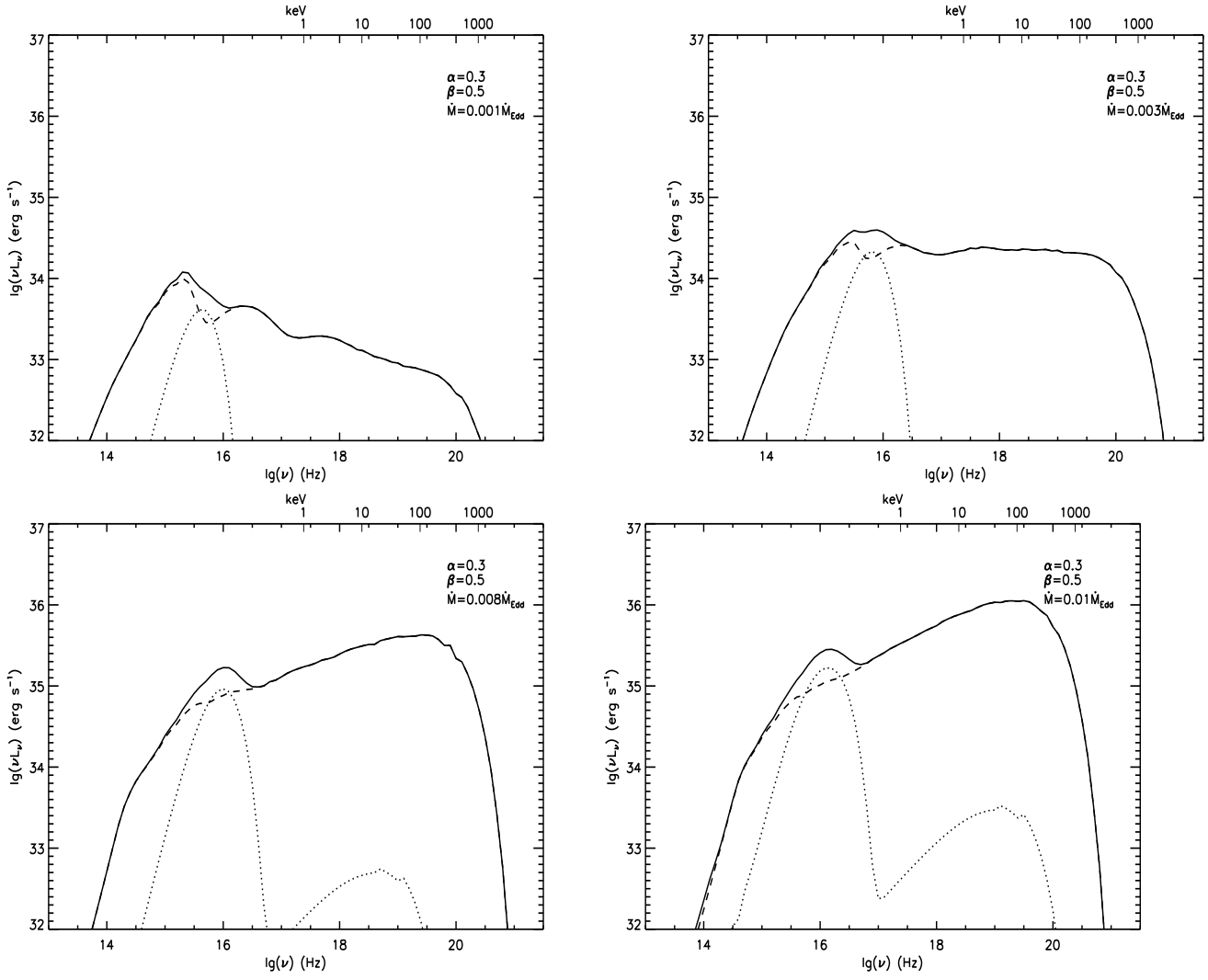


Fig. 5. The emergent spectra of disk and corona with mass evaporation for different mass accretion rates $\dot{M} = 0.001, 0.003, 0.008, 0.01 \dot{M}_{\text{Edd}}$. In each plot, the dashed line is the spectra of the inner ADAF and the dotted line is the spectra of the outer disk-corona. The solid line is the sum. $M = 6M_{\odot}$, $\alpha = 0.3$ and $\beta = 0.5$ are adopted.

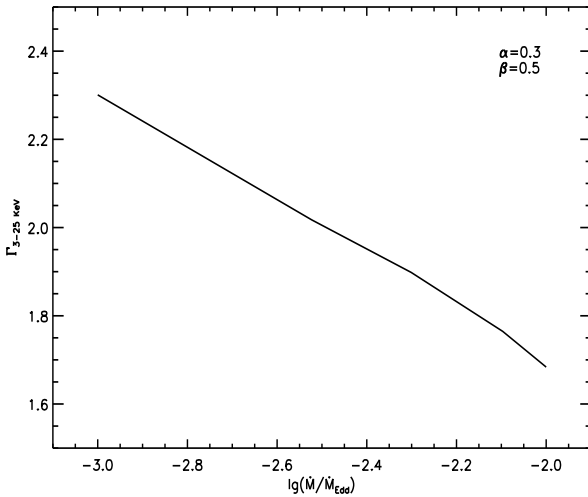


Fig. 6. The dependence of the hard X-ray photon index on the mass accretion rate. $M = 6M_{\odot}$, $\alpha = 0.3$ and $\beta = 0.5$ are adopted.

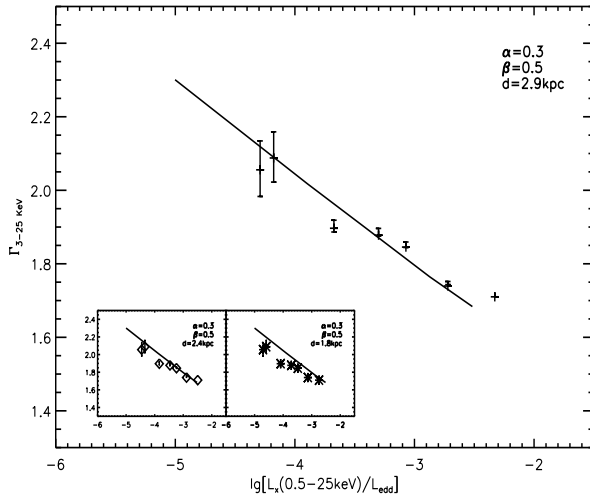


Fig. 7. The anti-correlation between the Eddington ratio ξ and the hard X-ray photon index $\Gamma_{3-25 \text{ keV}}$. The solid line are our theoretical prediction assuming $M = 6M_{\odot}$, $\alpha = 0.3$, $\beta = 0.5$. The pluses denote the observational data of X-ray source XTE J1118+480 for distance $d = 2.9 \text{ kpc}$. The diamonds in the first inset are for $d = 1.8 + 0.6 \text{ kpc}$, and the asterisks in the second inset are for $d = 1.8 \text{ kpc}$.